Near Surface Geophysics, 2014, **12**, 721-730 doi:10.3997/1873-0604.2014026

Estimating location of scatterers using seismic interferometry of scattered rayleigh waves

A. Kaslilar[1*], U. Harmankaya[1], K. van Wijk[2], K. Wapenaar[3] and D. Draganov[3]

[1] *Department of Geophysical Engineering, Faculty of Mines, Istanbul Technical University, 34469, Istanbul, Turkey*
[2] *Department of Physics, University of Auckland, New Zealand*
[3] *Sec. Applied Geophysics and Petrophysics, Dept. of Geoscience and Engineering, Delft University of Technology, The Netherlands*

Received October 2013, revision accepted April 2014

ABSTRACT

From non-destructive testing to medical imaging and seismology, estimating the location of scatterers is of high importance. The location estimation can be achieved using a method inspired by seismic interferometry. This method correlates only the isolated scattered fields from a scatterer, and inverts for the travel times to estimate the scatterer's location. The correlation eliminates the influence of the path between a source and a scatterer. We illustrate the potential of the method using data from a scaled laboratory model, representing geophysical field problems. We use ultrasonic data recorded on an aluminum block containing many scatterers at the surface represented by vertical drill holes. To estimate the horizontal coordinates of a scatterer, we use the scattered Rayleigh-wave fields recorded along two lines due to one source. We address the problem of selecting scattered fields along the two lines that pertain to the same scatterer using simple geometrical considerations, but also during the inversion. We show that the inversion does not converge when scattered fields coming from different scatterers have been chosen for the correlation.

INTRODUCTION

As near-surface scatterers may form weak zones and may pose risk for the environment, the investigation and detection of these structures is important for the mitigation of geo- and environmental hazards. Several geophysical methods, like electrical resistivity, electromagnetics, seismics, gravity, GPR, are available for obtaining the image of the subsurface and detecting scatterers. In seismic methods, one alternative for detecting near-surface scatterers is the exploitation of scattered seismic waves. Natural (karstic cavities) and man-made (mine shafts, tunnels, ruins) near-surface structures may cause scattering, when the scatterer's length scale is comparable to the dominant seismic wavelength. These scattered waves can be used for location and characterization of scatterers. Because of this, different studies have been performed that made use of scattered body and surface waves (e.g., Snieder 1987; Herman *et al*. 2000; Leparoux *et al*. 2000; Campman *et al*. 2004; Gelis *et al*. 2005; Grandjean and Leparoux 2004; Rodríguez-Castellanos *et al*. 2006; Campman and Riyanti 2007; Kaslilar 2007; Xia *et al*. 2007; Mohanty 2011; Chai *et al*. 2012; Harmankaya *et al*. 2013; Kaslilar *et al*. 2013).

In this paper, we use a method inspired by seismic interferometry and apply the method to scattered surface waves to estimate the location of scatterers. Seismic interferometry is a method that obtains new seismic responses (Green's functions) by cross-correlating (but also convolving or deconvolving) passive or controlled-source wavefields recorded at two receivers (Schuster *et al*. 2004; Snieder 2004; Wapenaar 2004). The result of seismic interferometry is that a response is retrieved at one of the receivers as if were a virtual source at the position of another receiver. This type of seismic interferometry is also called inter-receiver interferometry (Wapenaar 2004; van Manen *et al*. 2006). Using source-receiver reciprocity, the same principle can be applied to recordings from two sources and one could retrieve the Green's function between them (also called inter-source interferometry, Curtis *et al*. 2009). The Green's function could also be retrieved between the locations of a source and receiver, where the receiver has not recorded the response from the source in question (also called source-receiver interferometry (Curtis and Halliday 2010; Halliday and Curtis 2010; Meles and Curtis 2013).

To obtain a complete Green's function between the receivers, boundary sources (primary or secondary) must effectively enclose the receivers (Barmin *et al*. 2013; Campillo and Paul 2003; Schuster *et al*. 2004; Wapenaar 2004). When this condition is not met, apart from the physical wavefield, ghost arrivals (also called non-physical or spurious events) will appear in the retrieved responses (Snieder *et al*. 2008; Halliday and Curtis 2009; Snieder and Fleury 2010; Meles and Curtis 2013). These arrivals are called like that since they do not correspond to an actual event between the points of measurement. Using stationary-phase analysis (e.g., Halliday and Curtis 2009) it can be

* kaslilar@itu.edu.tr

shown that the ghost arrivals result from the correlation of direct with scattered wavefields and from the correlation of scattered with scattered wavefields. The two correlation results will interact destructively in the consecutive summation step and the ghost events will be suppressed or completely eliminated. This means that when only scattered wavefields are correlated, ghost events will always be present in the retrieved result. If there is an insufficient number of boundary sources, the ghost events may be prevalent. In an extreme case where only one boundary source is used and only scattered fields are correlated, it is very unlikely that any physical energy will be retrieved. In this paper, we exploit the latter fact and use only scattered arrivals from a single source for estimating the location of scatterers.

We utilize the method given in Harmankaya *et al.* (2013), which is inspired by active-source, inter-receiver seismic interferometry by cross-correlation. For the application of the method, only one active source is sufficient. By cross-correlating scattered surface waves only, ghost scattered arrivals are retrieved, and their arrival times are subsequently used in inversion for location purposes. When the correlations between the scattered wavefields are considered, the path from the source to the scatterer is eliminated. As the location of the scatterer does not change, the arrival times from the scatterer to receivers is always constant (stationary), irrespective of the source location.

We apply the method to an ultrasonic laboratory data (Mikesell *et al*. 2012) representative of geophysical field problems. The data are collected on an aluminum block with holes acting as scatterers. By considering the geometry of the ultrasonic data, we modify the method given by Harmankaya *et al*. (2013) to be able to locate scatterers not inline with the receiver line. We use recordings of the Rayleigh waves along two parallel and orthogonal lines of arrivals from the multiple scatterers due to one source and successfully estimate the location of scatterers.

In the following section, we explain the method. In section 3, the estimation of location of scatterers not inline with the receiver lines is shown. The discussions and conclusions are given in sections 4 and 5, respectively.

METHOD

We utilize the method from Harmankaya *et al*. (2013) modified for location of scatterers not aligned with a receiver line. We apply seismic interferometry to the recordings at a receiver array due to one active source. From an isolated scattered wavefield recorded along a line, we select a reference receiver as a virtual source (VS) and cross-correlate all the traces of the line (d^i) with the trace at the VS location (d^{VS}). This relation is given as

$$C_{d^i d^{VS}}(\tau) = \sum_n d^i(t_n)\, d^{VS}(t_n + \tau). \quad (1)$$

As one active source is sufficient for the application of the method, a summation over sources is not required contrary to the seismic-interferometry relation for retrieval of physical arrivals. The cross-correlation in equation (1) eliminates the common travel-path from the source to the scatterer and results in the retrieval of ghost scattered body or surface waves. The travel time of these ghost arrivals for a point scatterer at location (*x, y, z*) is given by

$$t_i = \frac{1}{V}\left\{\left[\left(x^i - x\right)^2 + \left(y^i - y\right)^2 + \left(z^i - z\right)^2\right]^{1/2} - \left[\left(x^{vs} - x\right)^2 + \left(y^{vs} - y\right)^2 + \left(z^{vs} - z\right)^2\right]^{1/2}\right\}, \quad (2)$$

where V is the wave velocity. Retrieval of the ghost scattered field for one virtual source is sufficient for locating the scatterer; however, more virtual sources can be used and the estimations can be compared and averaged.

The considered problem is weakly nonlinear in the unknown positions (x, y, z), therefore we linearize the problem and solve it iteratively. The linearized system of equations for the forward problem is denoted in matrix-vector form as $\Delta\mathbf{d} = \mathbf{G}\Delta\mathbf{m}$. The vector $\Delta\mathbf{d} = \mathbf{t}^{obs} - \mathbf{t}^{calc}$ is the difference between an observed non-physical arrival time, t^{obs}, and a calculated one, t^{calc}, on the basis of an assumed scatterer position, (equation 2). The unknown model parameters, i.e. the coordinates of the scatterer, are denoted by the vector $\Delta\mathbf{m}$, while the Jacobian (sensitivity) matrix is represented by $\mathbf{G}$. For the solution of the inverse problem we use the damped Singular Value Decomposition, as

$$\Delta\mathbf{m} = \mathbf{V}\Lambda\left(\Lambda^2 + \beta^2\mathbf{I}\right)^{-1}\mathbf{U}^T\Delta\mathbf{d}, \quad (3)$$

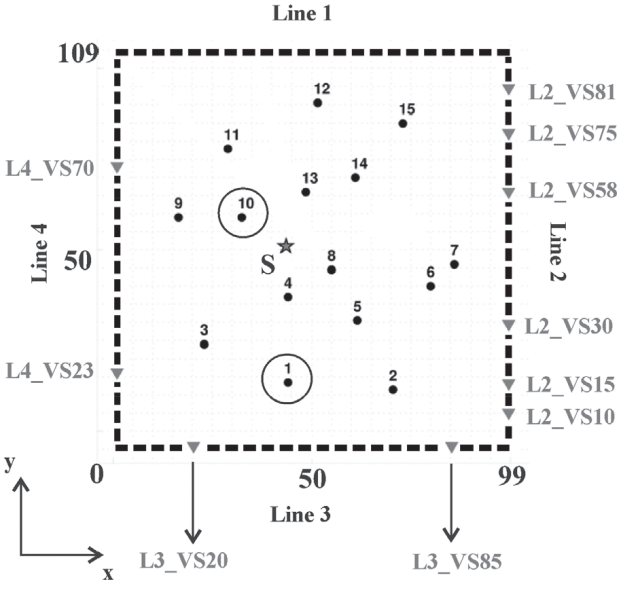

FIGURE 1

Top view of the ultrasonic laboratory set up: the source (star), receivers (dotted line) and scatterers (dots). The triangles are the virtual-source locations with the related short hand notations (see text). The scatterers whose locations are estimated are given in circles (1 and 10). The left bottom corner is set as the origin of the acquisition geometry.

where **V**, **Λ**, **A**, **U**, **I** and β are the model-space eigenvectors, the diagonal matrix containing the eigenvalues, the data-space eigenvectors, the identity matrix and the damping parameter, respectively. The damping parameter is chosen close to the lowest non-zero singular value. The uncertainties of the estimations are calculated by the model covariance matrix given as

$$\mathrm{cov}[\mathbf{m}] = \sigma^2 \mathbf{V} \Lambda^2 \left(\Lambda^2 + \beta^2 \mathbf{I}\right)^{-1} \mathbf{V}^{\mathrm{T}}, \tag{4}$$

where

$$\sigma^2 = \frac{1}{n - n_m} \sum_{k=1}^{n} \left(t_k^{obs} - t_k^{calc}\right)^2. \tag{5}$$

In equation (5), n is the number of arrival-time data and n_m is the number of model parameters. The square root of the diagonal values of the model covariance matrix, cov[m] (equation 4), is used to calculate the uncertainties of the estimations. A coverage factor 2 is considered, providing a level of 95% confidence (1.96σ).

The degree of agreement between the observed (t^{obs}) and the calculated travel times (t^{calc}) for the estimated model parameters are given by the following relation:

$$E_t = \frac{\sum_{k=1}^{N} (t_k^{obs} - t_k^{calc})^2}{\sum_{k=1}^{N} \left(t_k^{calc}\right)^2} \mathrm{x}100\,, \tag{6}$$

while the errors in the estimated model parameters are calculated by

$$E_m = \left| \frac{m_{act} - m_{est}}{m_{act}} \right| \mathrm{x}\,100\,, \tag{7}$$

where m_{act} and m_{est} are the actual and estimated model parameters, respectively, and they take the values of *x, y, and z*.

ESTIMATION OF THE LOCATION OF SCATTERERS

We apply the method to a part of an ultrasonic dataset (Fig. 1). It represents recordings along four receiver lines (dotted lines) with sampling of 1 mm from a source at S (the star). The recordings consist of direct and scattered Rayleigh-wave arrivals due to 15 scatterers (the dots). The left bottom corner is set as the origin of the acquisition geometry. The data are collected on an aluminum block with the irregularly located scatterers being cylindrical holes with a diameter of 1 mm and depth of 30 mm. The Rayleigh velocity in aluminum is 2900 m/s and the dominant frequency is 600 kHz, which gives a dominant wavelength of about 5 mm. This means that the scatterers (1 mm) are in the order of the dominant wavelength and the incident waves are scattered with large angles relative to the direction of the incident wavefield (Wu and Aki 1988).

This dataset was previously used by Mikesell *et al*. (2012), also to estimate the location (x and y coordinates) of the scatterers. The authors did that by autocorrelating the recordings at the receivers from the source at S, followed by summation over the receivers. The result was the retrieval of the complete Green's function that would be recorded using a source and receiver collocated at S. As the authors aimed for the retrieval of physical arrivals, they required an enclosing receiver boundary (all four lines) and the correlation of the complete wavefield (direct and scattered).

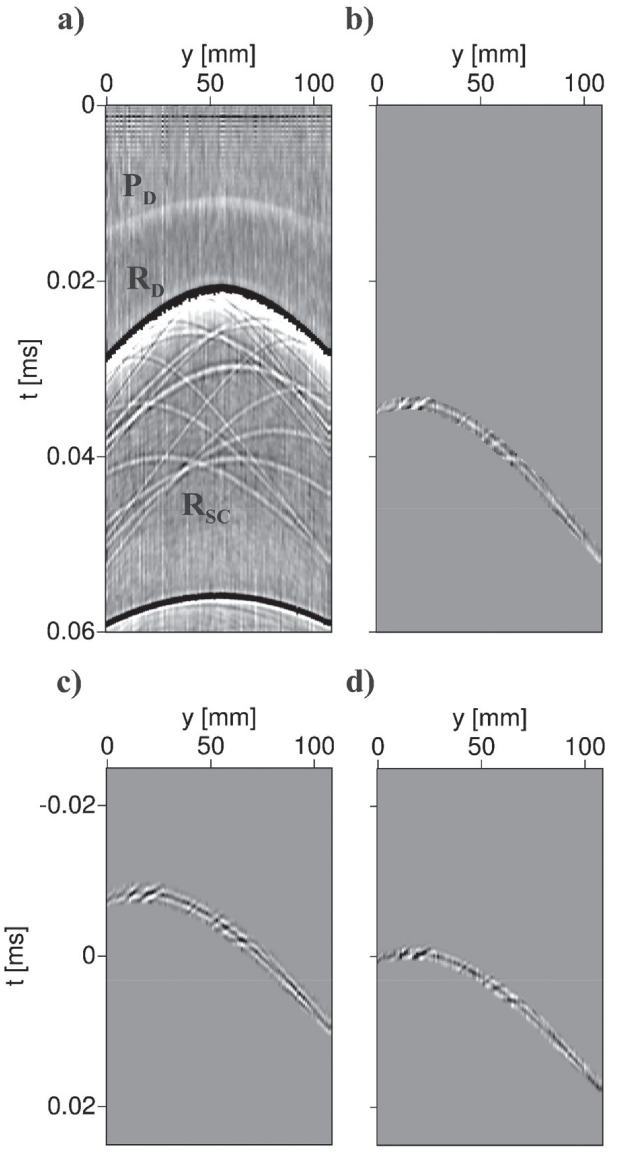

FIGURE 2
(a) Recorded wavefields along Line 2 due to the source at S. The direct compressional (P_D) and Rayleigh (R_D) waves and the scattered wavefields due to the scatterers (R_{SC}) are clearly observed. (b) Selected primary scattered Rayleigh-wave arrival due to a scatterer (scatterer 1 in Fig. 1). Ghost arrivals retrieved by seismic interferometry applied to (b) for the virtual sources at (c) VS75 and (d) VS30.

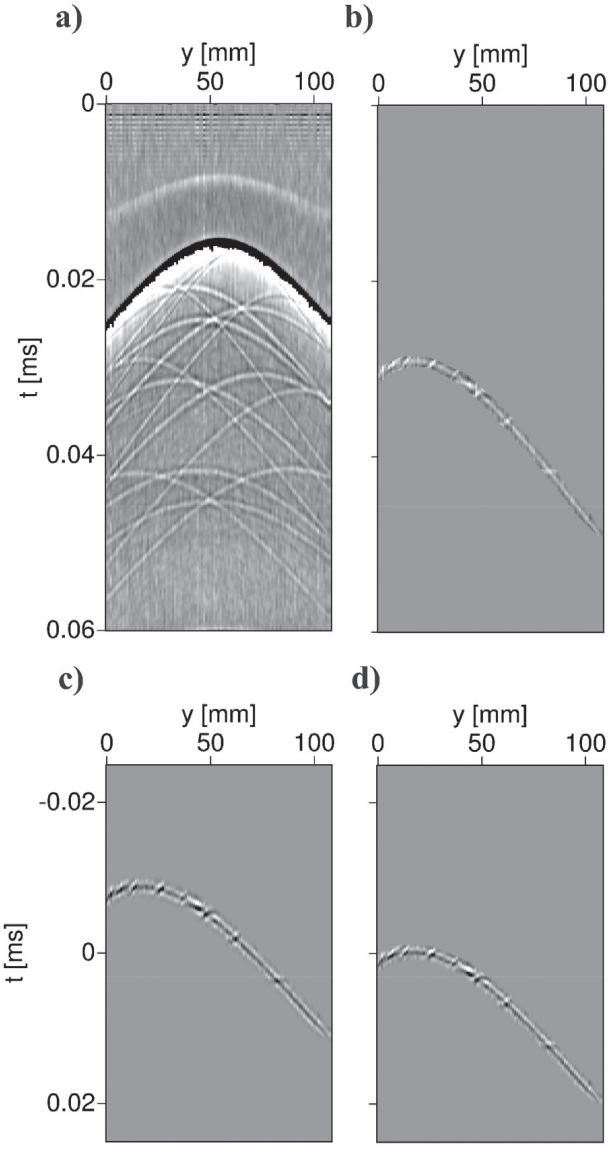

FIGURE 3
(a) and (b) as in Fig. 2, but along Line 4. (c) and (d) as in Fig. 2, but for VS70 and VS23, respectively.

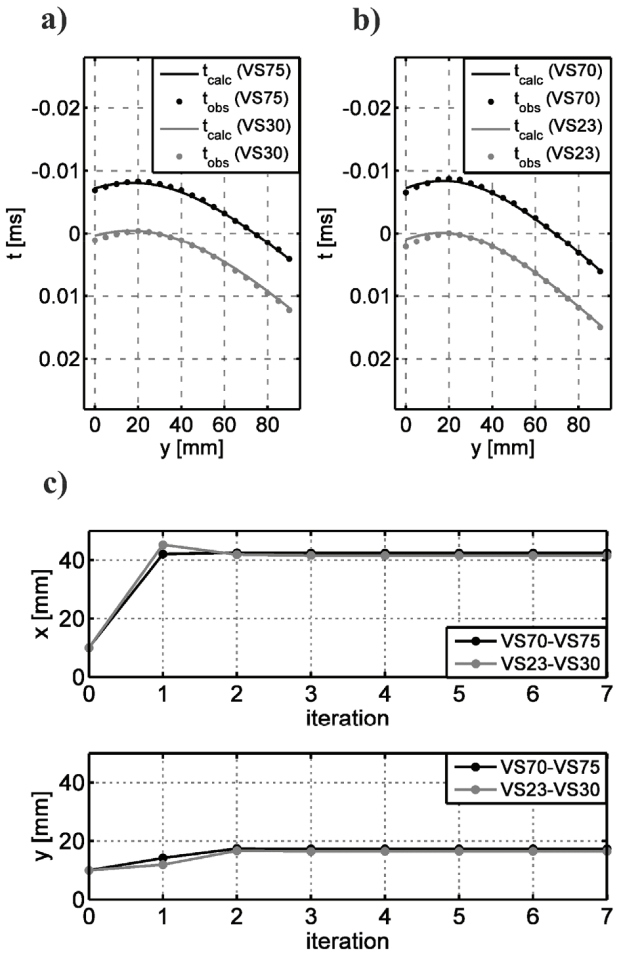

FIGURE 4
(a) and (b) Observed (dots) and calculated (solid line) travel times; (c) Estimated horizontal locations (x and y) of the scatterer for the virtual sources couples. The values at the zeroth iteration correspond to the initial parameters for the inversion.

Our method could be seen as an effective alternative, which imposes fewer restrictions on the measured dataset: it can work with irregular distribution of receivers provided that the scattered wavefield is isolated from the total wavefield. Here we consider an open receiver boundary and use the parallel receiver lines 2 and 4 in Fig. 1. The receivers denoted by triangles represent the VS locations that are used in the processing. Their shorthand notations are given next to the triangles, such that L2_VS75 indicates line 2 (L2) and the VS at receiver 75. The scatterers with circles are the ones whose locations are estimated after the application of our method.

To locate the x- and y-coordinate of the scatterer with scattered Rayleigh waves (Figs 2a and 3a) we use the following procedure. We select at both receiver lines the primary scattered arrivals that correspond to the same scatterer (Figs 2b and 3b). This is achieved using the fact that the aluminum block is homogeneous and thus the scattering arrivals will have their apexes around the same receiver locations along both lines. Then we isolate the scattered arrivals of interest by muting everything earlier and later in time. After that, we choose VS locations, for which we want to retrieve the ghost scattered waves needed for the inversion. We use VS75 and VS30 for L2 and VS70 and VS23 for L4 (Fig. 1).

For each VS location, the trace at that receiver is cross-correlated with all the traces of the muted scattered wavefield, including itself. In this way, the ghost scattered surface waves are retrieved (Fig. 2c-d and Fig. 3c-d). The correlation of the trace at the virtual-source location with itself results in a retrieved ghost arrival at time t = 0 s, whereas the arrivals at the other traces are shifted in agreement with equation (1).

To perform the inversion, the travel times are picked by considering the maximum amplitude of the retrieved ghost arrivals (dots in Fig. 4a and 4b), because the cross-correlation gives the maximum peak of the wavelet at the lag-time, where maximum similarity is obtained. Since two receiver lines are used for estimating the location of a scatterer, the matrix-vector form of the forward problem is rewritten as

$$\left[\Delta \mathbf{d1} \quad \Delta \mathbf{d2}\right]^{\mathbf{T}} = \left[\mathbf{G1} \quad \mathbf{G2}\right]^{\mathbf{T}} \Delta \mathbf{m}\,, \tag{8}$$

where 1 and 2 correspond to each receiver line with the same variables explained before and T representing transpose. The travel time inversion is performed for the couples L2_VS75-L4_VS70 and L2_VS30-L4_VS23. The estimation results for scatterer 1 are given in the first two rows of Table 1. The third row gives the average value of the couples. The updates of the model parameters after each iteration are given in Fig. 4c. The inversion is stopped when the changes in the model parameters become less than 0.1%. In our case, this also provides the best misfit in the data. In (noisy) field data, errors may warrant a more conservative stopping criterion (van Wijk *et al*. 2002). The picked (observed) ghost travel times are plotted together with the calculated ones in Fig. 4a for L2_VS75-30 and in Fig. 4b for L4_VS70-23. The comparison shows that there is a good agreement between the observed and the calculated travel times (Fig. 4a and b). This agreement is quantified by equation 6 and the results are given in Table 1. For scatterer 1, these errors are less than 1%. The errors in the estimated model parameters are calculated by equation 7. When the estimated coordinates given in Table 1 are compared to the actual coordinates of scatterer 1, it can be seen that the errors are less than 6%, and the average of errors are less than 3.5%.

We apply the above procedure also by using two orthogonal lines, L2 and L3, and we estimate the location of scatterer 10 (Fig. 1). The records of L2 and L3 due to source at S are given in Fig. 5a and 5b, while the selected and muted scattering fields are given in Fig. 5c and 5d, respectively. The travel time inversion is performed for the couples L2_VS15-L3_VS85 and L2_VS58-L3_VS20, and the results are listed in Table 1. From the results in Table 1, we can conclude that for both the parallel- and orthogonal-line geometries the locations of the scatterers are estimated with less than 6% error, and there is less than 1% error in the observed and the calculated travel times. For the orthogonal geometry, as long as the correct hyperbolas are selected, it is obvious that, exploiting the apices along the x and y axes, a rough estimation of the location of scatterer 10 can be obtained. However, when the scatterers are buried, the apices alone will not be sufficient to estimate the z coordinate. In this case also the travel-time readings along the slope of the branches of scattering hyperbolas will become important, since the slope is determined by the depth and the horizontal distance to the receiver line.

When a single scatterer or a small number of scatterers are present in the medium, the selection of the scattering hyperbolae is relatively straightforward. In a recent paper we show the application of the method to field seismic data where a single scatterer, an *a priori* known tunnel, is present in the medium (Kaslilar *et al*. 2013). However, if many scatterers are available, as in the laboratory data we use, it might be difficult to find the correct hyperbola at two receiver lines that belong to the same scatterer. We explained above that when using two parallel lines, the difficulty could be overcome by using simple geometrical considerations. The difficulty, though, is exacerbated in the case of orthogonal-lines geometry, as in this case the apexes of the hyperbolae are not around the same receiver location (as for the parallel-lines geometry). Nevertheless, also here there can be a practical solution. In case we select along each of the orthogonal lines hyperbolae that correspond to different scatterers, the observed and the calculated travel time curves will not match. This would be an indication that the hyperbolae are not representing the same scatterer.

TABLE 1

The estimated model parameters for different records (Line #) and virtual-source (VS #) locations for the configuration given in Fig. 1. The actual location of the scatterer (AL), the estimated parameters (x and y) with their 95% confidence levels (1.96 σ), percentage errors on the travel times (E_t) and model parameters (E_m) are also given.

Line #	VS #	AL [mm] x / y	$x\pm\sigma_x$ [mm]	$y\pm\sigma_y$ [mm]	E_t	E_m x / y
			Scatterer 1			
2-4	75-70		42.50±0.98	17.32±0.41	0.15	1.2/1.0
2-4	30-23	43.0/17.5	41.57±1.57	16.49±0.80	0.34	3.3/5.8
Average			42.03±1.31	16.90±0.62		2.3/3.4
			Scatterer 10			
2-3	15-85		30.60±0.33	62.70±0.40	0.08	2.9/1.3
2-3	58-20	31.5/63.5	29.71±0.53	63.42±0.73	0.30	5.7/0.1
Average			30.15±0.43	63.06±0.59		4.3/0.7

When it is not possible to determine the scattering hyperbolas that correspond to the same scatterer, a practical tool can be the extension of the latter method. Assume that along one of the receiver lines one isolates all scattered wavefields, while along the other receiver line only one scattered wavefield is isolated. By keeping the latter one fixed, one can invert for scatterer locations by using scattered arrivals from the former record. For each couple of scattering hyperbolas, the inversion will stop when the model-parameter variation has no significant improvement on the model. At this stage, one should keep the misfit value for each couple. After the inversions are finalized for the different couples, we expect the minimum misfit will be obtained when the hyperbolas correspond to the same scatterer. After eliminating the two hyperbolas which are already used in the location of a scatterer, the procedure can be repeated for another isolated hyperbola and the location of another scatterer can be estimated. To illustrate this, we select a reference hyperbola along Line 4 (Fig. 3b) which we know that corresponds to scatterer 1, but assume we do not know that. Along line 2 we select the scattering hyperbolas numbered in Fig. 6a and isolate them (Fig. 6 b-e). By keeping the hyperbola from Line 4 fixed, we invert for the selected lines the travel times for virtual-source couples L4_VS70 & L2_VS75 (Fig. 7), L4_VS70 & L2_VS58 (Fig. 8), L4_VS70 & L2_VS10 (Fig. 9), and L4_VS70 & L2_VS81 (Fig. 10). In Fig. 7, the hyperbolas from Line 2 and Line 4 correspond to scatterer 1. Therefore the calculated and observed traveltimes are in good agreement (E_t < 1%) and the model parameters are estimated with less than 2% error (Table 2, first row). In Fig. 8, we illustrate the results when using along Line 2 the hyperbola 2 (Fig. 6c) that does not correspond to scatterer 1. As can be seen in Fig. 8a-b the agreement between the observed and the calculated travel times is too poor to permit us to accept the estimated parameters as a solution to the inversion. For this couple, the errors in the travel time are 53% and the errors in the model parameters for x and y locations are 54% and 69%, respectively. In Fig. 9, we use along Line 2 hyperbola 3 (Fig. 6c) in the inversion. The apex of this hyperbola is close to the apex of the hyperbola given in Fig. 3b (reference hyperbola), however, they do not correspond to the same scatterer, i.e. scatterer 1, instead the hyperbola in Fig. 6c corresponds to scatterer 3 (Fig. 1). When we invert for the travel times, we obtain a good agreement in the travel times, 1.25% error, however, the error in the model parameters x and y are 45% and 46%, respectively (Table 2, row 3). In Table 2, when the error in the travel times of hyperbola 3 is compared with hyperbola 1, we observe that the minimum error is obtained when the hyperbolas correspond the same scatterer. In Fig. 10a-b, again, we observed a traveltime fit that cannot be accepted as the solution (Table 2, row 4). When Figs 7c-10c are examined, we observe that when the shape of scattering hyperbolas differ from each other, the update in the model parameters oscillates; this is not observed when the hyperbolas are similar.

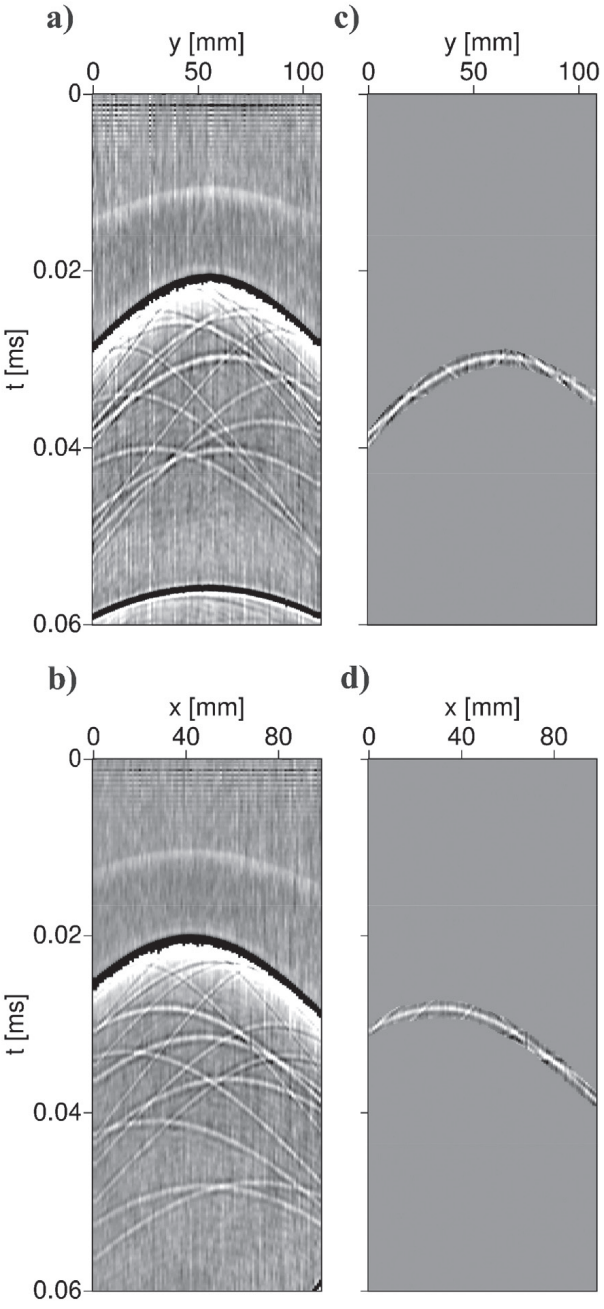

FIGURE 5
Recorded wavefields from the source at S along (a) Line 2 and (b) Line 3. Selected primary scattered Rayleigh-wave arrival along (c) Line 2 and (d) Line 3.

DISCUSSIONS

We show the potential of the method proposed by Harmankaya *et al*. (2013) to estimate the location of scatterers that are offline to the receiver lines. We use ultrasonic data and show that two receiver lines are sufficient to estimate the location of an offline scatterer. When complete (physical) Green's function retrieval of the scatterer is not the primary purpose, but the estimation of the

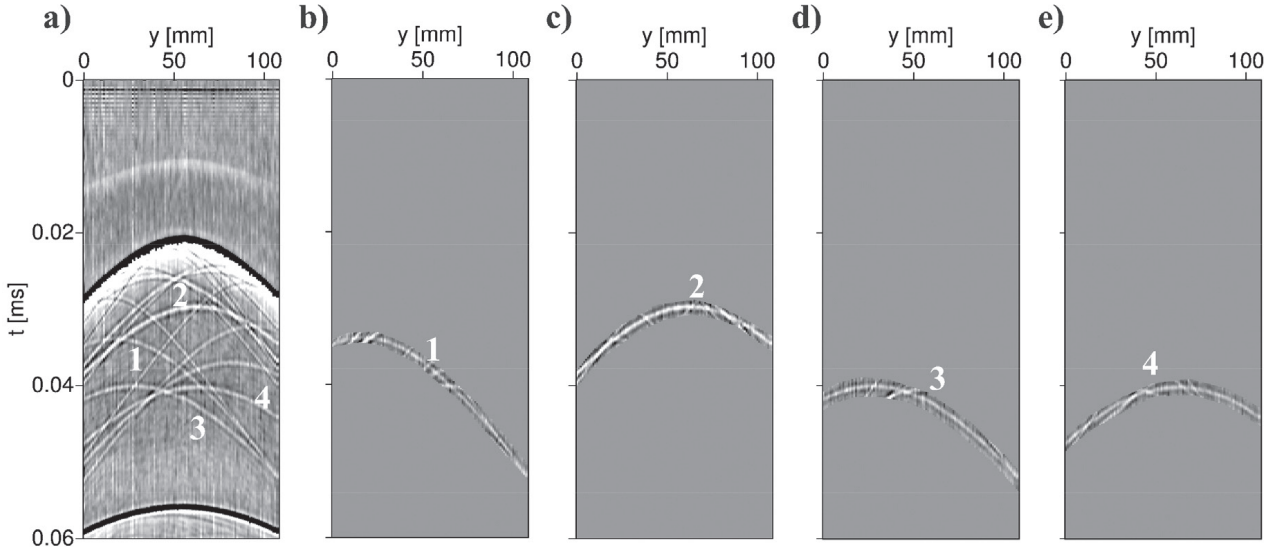

FIGURE 6

(a) Scattering hyperbolas along Line 2. (b-e) Isolated hyperbolas corresponding to the events in (a) labelled from 1 to 4.

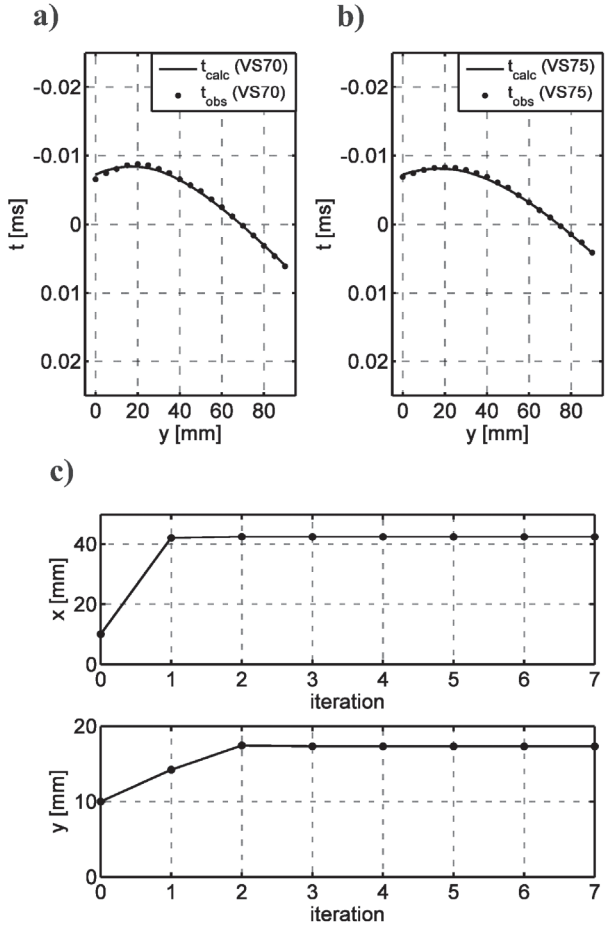

FIGURE 7

Observed (dots) and calculated (solid line) travel times for (a) L4_VS70 and (b) L2_VS75; (c) Estimated horizontal locations of the scatterer for the selected lines and virtual sources couples.

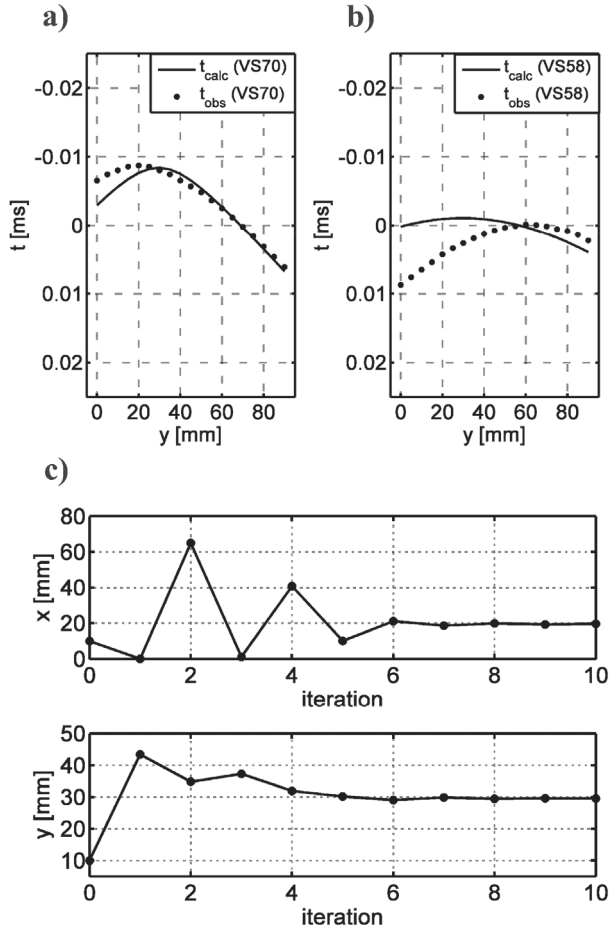

FIGURE 8

(a), (b) and (c) same as in Fig. 7, but for L4_VS70 and L2_VS58, respectively.

TABLE 2
Same as Table 1. H stands for hyperbola.

H	Line #	VS #	AL [mm] x / y	$x\pm\sigma_x$ [mm]	$y\pm\sigma_y$ [mm]	E_t	E_m x / y
				Scatterer 1			
1	2-4	75-70	43.0/17.5	42.50±0.98	17.32±0.41	0.15	1.2/1.0
2		58-70		19.62±9.72	29.54±3.23	52.85	54.4/68.8
3		10-70		23.83±1.36	25.50±0.45	1.25	44.6/45.7
4		81-70		22.19±12.15	31.19±3.61	74.83	48.4/78.2

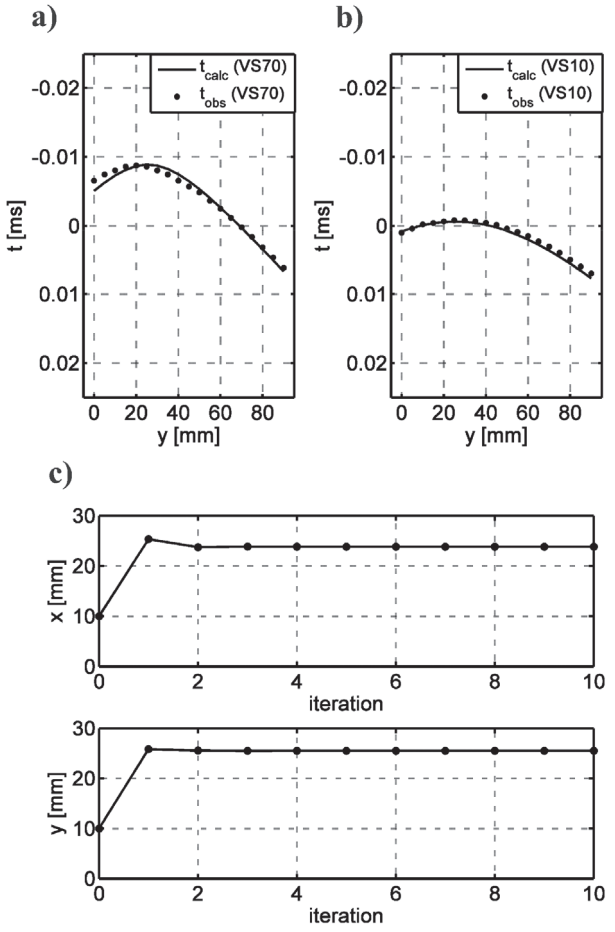

FIGURE 9
(a), (b) and (c) same as in Fig. 7, but for L4_VS70 and L2_VS10, respectively.

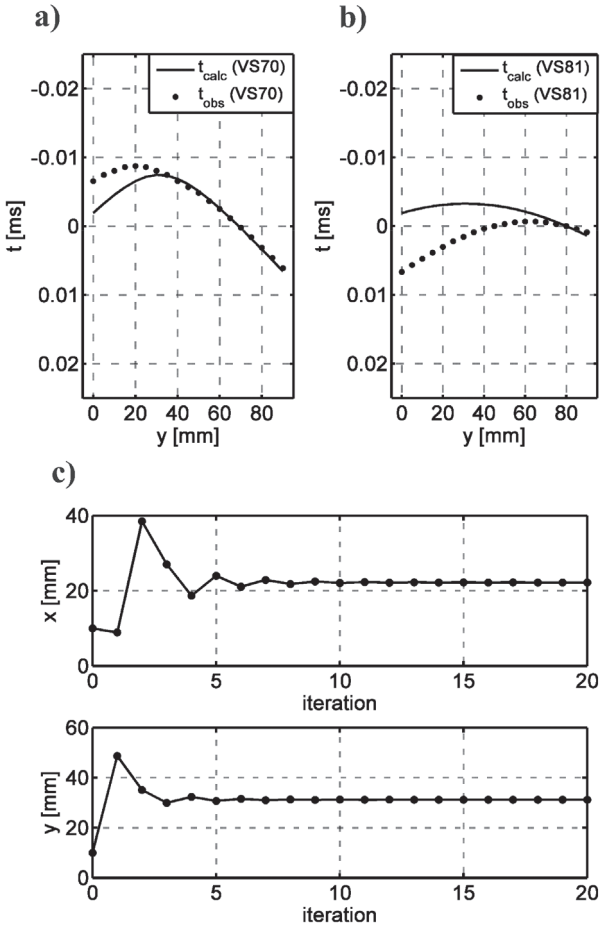

FIGURE 10
(a), (b) and (c) same as in Fig. 7, but for L4_VS70 and L2_VS81, respectively.

location of a scatterer, this method can be an effective alternative, since it works with an open receiver boundary.

The quality of the estimations depends on the quality of the isolated scattered wavefields from the total wavefield, and the correct travel time picks. If a virtual source is created at a trace where the scattered surface-wave arrival has been strongly suppressed, the retrieved ghost scattered surface waves in this virtual-source gather would be of a poor quality. As a consequence, application of the inversion step to this gather might result in a poor estimation of the scatterer parameters therefore such results should be treated as outliers.

In the ultrasonic data set, the isolation of the scattered wavefield is relatively easy, since some of the scatterers are located sufficiently off to the side of the receiver line, and the isolation is provided by muting the scattered wavefield. In case of inline scatterers with receiver lines, application of a matched or f-k

filtering will be appropriate for isolating the scattered wavefield. When lateral and vertical inhomogeneities are present in the medium, but it is possible to extract the scatterered wavefield, we can successfully apply the method and estimate the locations of the scatterer. Examples of such cases are given in (Harmankaya *et al*. 2013, Figs 12–15)

In our experiment the scatterers are at the surface, therefore we estimate x and y coordinates of the scatterers. In the case of a buried scatterer, estimating the depth of the scatterer is straightforward using equation (1). Numerical and field data examples of buried single scatterers in line with a receiver line are given in Harmakaya *et al*. (2013) and Kaslilar *et al*. (2013), respectively.

The method is based on point-scatterer assumption, and there may be situations where the scatterers may not be considered to be point scatterers. Nevertheless, the boundaries of the scatterers will act as points, so using the scattered wavefield from that boundary will allow information about the scatterer to be estimated.

For the inversion, we considered the wave velocity as a known parameter, which can be estimated from the direct arrivals of a seismic record. Instead, one might decide to include the velocity as an unknown parameter in $\Delta\mathbf{m}$ and to estimate it together with the scatterer location. However, to avoid the difficulties of the multi-parameter inversion and to increase the accuracy of the estimation of the locations, we prefer to keep the velocity as a known parameter.

CONCLUSIONS

Correlating the scattered Rayleigh waves at different receiver locations provides the necessary information to locate the scatterers. An open boundary of receivers, in this case two lines of receivers, is sufficient to locate the scatterers, provided that the scattered wave fields selected from the two receiver lines are representing the same scatterer and are well isolated from the total wave field. In case of a single receiver line located to one side of the scatterer, the location estimations are still possible with less accuracy. An important advantage of the presented technique is that the method is independent of the wave propagation from the source to the scatterer. As a result, we foresee application in wave-scattering problems from engineering to global scale.

ACKNOWLEDGEMENTS

This work is supported by TUBITAK (The Scientific and Technological Research Council of Turkey) with the project CAYDAG-110Y250. A.K and U.H. gratefully acknowledge this financial support. The investigations of D.D. are supported by the Division for Earth and Life Sciences (ALW) with financial aid from the Netherlands Organization for Scientific Research (NWO).

REFERENCES

Campman X., van Wijk K., Riyanti C.D., Scales J. and Herman G. 2004. Imaging scattered seismic surface waves. *Near Surface Geophysics* **2**(4), 223–230.

Campman X. and Riyanti C.D. 2007. Non-linear inversion of scattered seismic surface waves. *Geophysical Journal International* **171**, 1118–1125, doi: 10.1111/j.1365-246X.2007.03557.x.

Chai H.Y., Phoon K., Goh S.H. and Wei C.F. 2012. Some theoretical and numerical observations on scattering of Rayleigh waves in media containing shallow rectangular cavities. *Journal Applied Geophysics* **83**, 107–119, doi: 10.1016/j.jappgeo.2012.05.005. ISSN: 0926-9851.

Curtis A. and Halliday D. 2010. Source-receiver wave field interferometry. *Physical Review E* **81**, 046601.

Curtis A., Nicolson H., Halliday D., Trampert J. and Baptie B. 2009. Virtual seismometers in the subsurface of the Earth from seismic interferometry. *Nature Geoscience* **2**, 700–704.

Gelis C., Leparoux D., Virieux J., Bitri A., Operto S. and Grandjean G. 2005. Numerical modeling of surface waves over shallow cavities. *Journal of Environmental & Engineering Geophysics* **10**(2), 111–121, doi:10.2113/JEEG10.2.111.

Grandjean G. and Leparoux D. 2004. The potential of seismic methods for detecting cavities and buried objects: experimentation at a test site. *Journal of Applied Geophysics* **56**(2), 93–106, doi: 10.1016/j.jappgeo.2004.04.004.

Halliday D.F. and Curtis A. 2009. Seismic interferometry of scattered surface waves in attenuative media. *Geophysical Journal International* **178**, 419–446, doi: 10.1111/j.1365-246X.2009.04153.x.

Halliday D.F. and Curtis A. 2010. An interferometric theory of source-receiver scattering and imaging. *Geophysics* **75**, SA95-SA103.

Harmankaya U., Kaslilar A., Thorbecke J., Wapenaar K. and Draganov D. 2013. Locating near-surface scatterers using non-physical scattered waves resulting from seismic interferometry. *Journal of Applied Geophysics* **91**, 66–81, doi: 10.1016/j.jappgeo.2013.02.004.

Herman G.C., Milligan P.A., Huggins R.J. and Rector J.W. 2000. Imaging shallow objects and heterogeneities with scattered guided waves. *Geophysics* **65**(1), 247–252.

Kaslilar A. 2007. Inverse scattering of surface waves: imaging of near-surface heterogeneities. *Geophysical Journal International* **171**, 352–367, doi: 10.1111/j.1365-246X.2007.03524.x.

Leparoux D., Bitri A. and Grandjean G. 2000. Underground cavity detection: a new method based on seismic Rayleigh Waves. *EJEEG* **5**, 33–53.

Meles A.G. and Curtis A. 2013. Physical and non-physical energy in scattered wave source-receiver interferometry. *Journal of the Acoustical Society of America* **133**(6), 3790–3801, doi: 10.1121/1.4802825.

Mikesell T.D., van Wijk K., Blum T.E., Snieder R. and Sato H. 2012. Analyzing the coda fromcorrelating scattered surface waves. *Journal of the Acoustical Society of America* **131**(3), EL275–EL281, doi: 10.1121/1.3687427.

Mohanty P.R. 2011. Numerical Modeling of P-Waves for Shallow Subsurface Cavities Associated with Old Abandoned Coal Workings. *Journal of Environmental and Engineering Geophysics* **16**(4), 165–175.

Rodríguez-Castellanos A., Sánchez-Sesma F.J., Luzón F. and Martin R. 2006. Multiple Scattering of Elastic Waves by Subsurface Fractures and Cavities. *Bulletin of the Seismological Society of America* **96**(4A), 1359–1374.

Schuster G.T., Yu J., Sheng J. and Rickett J. 2004. Interferometric/daylight imaging, *Geophysical Journal International* **157**, 838–852 doi:10.1111/j.1365-246X.2004.02251.x.

Snieder R. and Nolet G. 1987. Linearized scattering of surface waves on a spherical Earth. *Journal of Geophysics* **61**, 55–63.

Snieder R. 2004. Extracting the Green's function from the correlation of coda waves: A derivation based on stationary phase. *Physical Review E* **69**, 046610, doi: 10.1103/PhysRevE.69.046610.

Snieder R., van Wijk K., Haney M. and Calvert R. 2008. Cancellation of spurious arrivals in Green's function extraction and the generalized

optical theorem. *Physical Review E* **78**, 036606, doi: 10.1103/PhysRevE.78.036606.

Snieder R. and Fleury C. 2010. Cancellation of spurious arrivals in Green's function retrieval of multiple scattered waves. *Journal of the Acoustical Society of America* **128**(4), 1598–1605.

van Manen D., Curtis A. and Robertsson J.O.A. 2006. Interferometric modeling of wave propagation in inhomogeneous elastic media using time reversal and reciprocity. *Geophysics* **71**(4), SI47–SI60.

van Wijk K., Scales J.A., Navidi W. and Tenorio L. 2002. Data and model uncertainty estimation for linear inversion. *Geophysical Journal International* **149**, 625–632.

Wapenaar K. 2004. Retrieving the elastodynamic Green's function of an arbitrary inhomogeneous medium by cross correlation. *Physical Review Letters* **93**(25), 254301, doi: 10.1103/PhysRevLett.93.254301.

Wu R.S. and Aki K. 1988. Introduction: Seismic wave scattering in three-dimensionally heterogeneous earth. *PAGEOPH* **128** (1/2), 1–5.

Xia J., Nyquist J.E., Xu Y.X., Roth M.J.S. and Miller R.D. 2007. Feasibility of detecting near-surface feature with Rayleigh-wave diffraction. *Journal of Applied Geophysics* **62**(3), 244–253, doi: 10.1016/j.jappgeo.2006.12.002.